Nonstandard Hubbard model and electron pairing

M. Zendra [1,2,3,*] F. Borgonovi [1,3] G. L. Celardo [4,5] and S. Gurvitz [6,†]

[1]*Dipartimento di Matematica e Fisica and Interdisciplinary Laboratories for Advanced Materials Physics, Università Cattolica del Sacro Cuore, via della Garzetta 48, 25133 Brescia, Italy*

[2]*Institute for Theoretical Physics, KU Leuven, Celestijnenlaan 200D, B-3001 Leuven, Belgium*

[3]*Istituto Nazionale di Fisica Nucleare, Sezione di Milano, via Celoria 16, I-20133 Milano, Italy*

[4]*Dipartimento di Fisica e Astronomia, Università di Firenze, via Sansone 1, 50019 Sesto Fiorentino, Firenze, Italy*

[5]*Istituto Nazionale di Fisica Nucleare, Sezione di Firenze, via Bruno Rossi 1, 50019 Sesto Fiorentino, Firenze, Italy*

[6]*Department of Particle Physics and Astrophysics, Weizmann Institute of Science, 76100 Rehovot, Israel*

(Received 21 September 2023; revised 22 April 2024; accepted 23 April 2024; published 10 May 2024)

We present a nonstandard Hubbard model applicable to arbitrary single-particle potential profiles and interparticle interactions. Our approach involves a treatment of Wannier functions, free from the ambiguities of conventional methods and applicable to finite systems without periodicity constraints. To ensure the consistent evaluation of Wannier functions, we develop a perturbative approach, utilizing the barrier penetration coefficient as a perturbation parameter. With the defined Wannier functions as a basis, we derive the Hubbard Hamiltonian, revealing the emergence of density-induced and pair tunneling terms alongside standard contributions. Our investigation demonstrates that long-range interparticle interactions can induce a mechanism for repulsive particle pairing. This mechanism relies on the effective suppression of single-particle tunneling due to density-induced tunneling. Contrary to expectations based on the standard Hubbard model, an increase in interparticle interaction does not lead to an insulating state. Instead, our proposed mechanism implies the coherent motion of correlated electron pairs, similar to bound states within a multiwell system, resistant to decay from single-electron tunneling transitions. These findings carry significant implications for various phenomena, including the formation of flat bands, the emergence of superconductivity in twisted bilayer graphene, and the possibility of a metal-insulator transition.

DOI: 10.1103/PhysRevB.109.195137

I. INTRODUCTION

Electron pairing in solids has traditionally been attributed to phonon-mediated attraction. However, a fundamental question is whether repulsive particles can form pairs independently of the presence of phonons. To explore this idea further, we examine two interacting electrons within the same site of a periodic structure, as described by the Hubbard model [1]. When the on-site two-particle repulsive energy, denoted as U, significantly exceeds the tunneling coupling Ω, *single-electron* hopping to a neighboring site is strongly suppressed due to the large energy mismatch. Concerning the tunneling of an electron pair, the *elastic* two-electron hopping (known as "cotunneling") is also suppressed in the standard Hubbard model. Indeed, the corresponding amplitude representing two consecutive hoppings is a second-order process that involves a large virtual energy variation $\sim 2\Omega^2/U$ [2], which decreases with U. Even if weak, this second-order process survives for any finite interaction U, so that the repulsive interaction cannot completely localize the electron pair within the framework of the standard Hubbard model.

However, it is evident that the standard Hubbard Hamiltonian fails to capture all the interaction effects [3–5]. For instance, the cotunneling process can occur with both particles staying together, without changing their total energy, a nonstandard Hubbard process known as pair tunneling (PT) [3]. Even with increasing U, the latter can become a major contributor to the cotunneling process [6]. Indeed, even in the case of single-electron tunneling coupling suppression ($\Omega \to 0$), PT remains uninhibited, offering an effective mechanism for electron pairing, independent of the attractive interaction. A similar idea was proposed by Anderson in the theory of cuprate superconductivity [7]. Inspired by this idea, we demonstrate how this specific mechanism can be realized within the framework of a nonstandard Hubbard model, which includes both the pair tunneling term and the density-induced tunneling (DT) term, also known as *bond-charge interaction* [3–5,8–15]. While the influence of the PT term on superconductivity is rather obvious, the effect of the DT term (with the adequate sign) also favors superconductivity. Indeed, analytical demonstrations have highlighted the role of this term in supporting the emergence of superconductivity within models characterized by repulsive on-site interaction at half filling [16]. Thus the DT and PT terms play a crucial role in electron dynamics, both in terms of their magnitude and sign. Specifically, we show that the DT term, in the presence of a long-range interparticle interaction, has the ability to lower

*Corresponding author: matteo.zendra@unicatt.it

†Corresponding author: shmuel.gurvitz@weizmann.ac.il

and even totally suppress the single-particle coupling, due to an effective mean-field generated by the other particles, thus providing stability of the electron pair.

An extension of the standard Hubbard model concerning strongly correlated systems has been explored long ago in [17]. However, only recently has the nonstandard Hubbard model attracted more attention, particularly due to experimental results with ultracold atoms in optical lattices [3,5,18–20], as well as because they have been shown to host many different effects, ranging from superconducting pairing to localization [21–29]. Currently, the accurate evaluation of nonstandard Hubbard terms and the understanding of their influence on the dynamics of correlated systems remain open problems. Indeed, these terms are closely related to the overlap of Wannier functions (WFs) from adjacent sites, often accurately represented by the corresponding orbital wave functions. However, their overlap, crucially dependent on their tails being situated in neighboring sites, significantly affects both the magnitude and sign of nonstandard Hubbard terms, on which consensus is yet to be reached [3,17,30].

In what follows, we present an approach for evaluating the WFs in a multiwell potential, based on the two-potential approach (TPA) to tunneling problems, originally developed for tunneling to the continuum [31–33], which allows for an accurate evaluation of nonstandard Hubbard terms. Specifically, after a proper definition of the WFs of a multiwell potential in Sec. II, we present the TPA in Sec. III and we apply it to the case of a triple-well potential in Sec. IV. Finally, in Sec. V we analyze the effect of the PT and DT terms, for both a contact interaction and a long-range constant interaction. Specifically, in Sec. V A we analyze the simple case of a square double-well potential, showing that the DT term can effectively suppress the total single-particle tunneling amplitude only in the presence of a long-range interaction. In Sec. V B, we study the dynamics of two electrons with parallel spins in a square triple-well potential. In particular, we show under which conditions the nonstandard DT and PT terms become significant and when the nonstandard Hubbard model should be used instead of the extended Hubbard model (which neglects DT and PT contributions).

II. WANNIER FUNCTIONS

Let us consider a particle placed in an N-site potential chain

$$\mathcal{V}(x) = \sum_{j=1}^{N} \mathcal{V}_j(x), \tag{1}$$

where $\mathcal{V}(x) \to 0$ as $x \to \pm\infty$. The exact eigenstates are obtained from the Schrödinger equation (we take $\hbar = 1$)

$$\mathcal{H}\,|\psi_k\rangle \equiv \left(-\frac{\nabla_x^2}{2m} + \mathcal{V}(x)\right)|\psi_k\rangle = \mathcal{E}_k\,|\psi_k\rangle\,, \tag{2}$$

with boundary conditions at infinity ($x \to \pm\infty$) given by

$$\psi_k(x) \sim e^{-\sqrt{-2m\mathcal{E}_k}|x|} \tag{3}$$

that uniquely define the bound state energy spectrum ($\mathcal{E}_k < 0$) of the exact Hamiltonian $\mathcal{H}$. We assume that the N lowest eigenstates form a band, well separated from the other eigenstates of the spectrum.

We consider the corresponding tight-binding tunneling Hamiltonian H_N, which describes the lowest band of the exact Hamiltonian $\mathcal{H}$, given by

$$H_N = \sum_{j=1}^{N} \overline{E}_j\,|\Psi_j\rangle\,\langle\Psi_j| + \sum_{j=1}^{N-1} \overline{\Omega}_j(|\Psi_j\rangle\,\langle\Psi_{j+1}| + \text{H.c.}), \tag{4}$$

where $\overline{E}_j$ represents the single-site energy, $\overline{\Omega}_j$ is the nearest neighbor tunneling coupling, while $\Psi_j(x) = \langle x|\Psi_j\rangle$ are the WFs. In order to define $\overline{E}_j$ and $\overline{\Omega}_j$ in a consistent way, we identify the spectrum of the tunneling Hamiltonian in Eq. (4) with the one of the lowest bands of the original Hamiltonian $\mathcal{H}$ in Eq. (2). When employing such a procedure, unlike when solving exactly the Schrödinger Eq. (2), we are neglecting the influence of interband transitions on electrons' motion. Indeed, if the lowest band is sufficiently separated from the other bands, the exact spectrum obtained from Eq. (2) and the one of the tunneling Hamiltonian will produce the same dynamics. Therefore, we diagonalize the Hamiltonian H_N by a unitary transformation R and then we apply the same transformation to the lowest-band spectrum, namely $\mathcal{E}_k$ and $|\psi_k\rangle$, to obtain the WFs. In particular, these are uniquely defined by

$$|\Psi_k\rangle = \sum_{k'=1}^{N} R_{kk'}\,|\psi_{k'}\rangle\,. \tag{5}$$

Notice that the exact eigenfunctions $\psi_k(x)$ do not contain uncertainty, as belonging to the bound-state spectrum of the Schrödinger Eq. (2). In the following, we will illustrate the unitary transformation given in Eq. (5) for the double-well and triple-well potential cases (for details, see the Supplemental Material [34]).

Let us exemplify this method considering the symmetric double-well potential $\mathcal{V}(x)$ in Fig. 1(a), where the lowest band contains two eigenstates $\psi_{1,2}(x)$, with corresponding eigenenergies $\mathcal{E}_{1,2}$. The tunneling Hamiltonian of this system is given by Eq. (4) for $N = 2$ and can be explicitly written as

$$H_2 = \overline{E}_0 \sum_{j=1}^{2} |\Psi_j\rangle\,\langle\Psi_j| + \overline{\Omega}_0(|\Psi_1\rangle\,\langle\Psi_2| + \text{H.c.}). \tag{6}$$

By diagonalizing H_2 through the unitary transformation R in Eq. (5), and identifying its eigenspectrum with $\mathcal{E}_{1,2}$ and $\psi_{1,2}(x)$, we find

$$\overline{E}_0 = \frac{1}{2}(\mathcal{E}_1 + \mathcal{E}_2), \quad \overline{\Omega}_0 = \frac{1}{2}(\mathcal{E}_1 - \mathcal{E}_2), \tag{7a}$$

$$\Psi_{1,2}(x) = \frac{1}{\sqrt{2}}[\psi_1(x) \pm \psi_2(x)]. \tag{7b}$$

In contrast with the "extended" eigenstates $\psi_{1,2}(x)$, the WFs $\Psi_{1,2}(x)$ are localized respectively in the left and right well, although their tails are extended to the neighboring wells.

This procedure can be easily extended for the symmetric triple-well potential ($N = 3$) in Fig. 2, where the lowest band consists of three eigenstates $\psi_{1,2,3}(x)$ with energies $\mathcal{E}_1 < \mathcal{E}_2 < \mathcal{E}_3$. The corresponding tight-binding tunneling Hamiltonian,

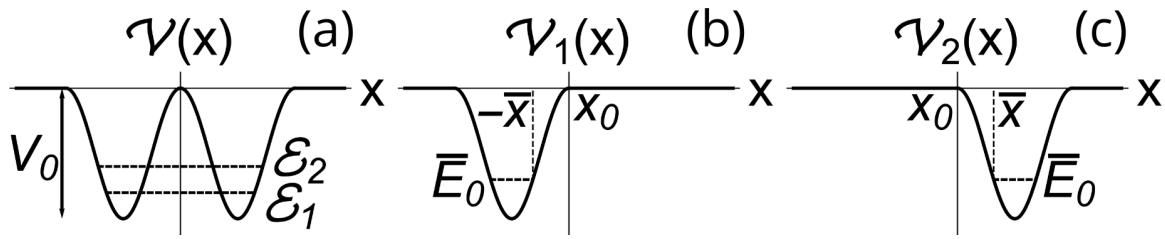

FIG. 1. (a) Symmetric double-well potential $\mathcal{V}(x) = \mathcal{V}_1(x) + \mathcal{V}_2(x)$, with lattice depth V_0. Dashed lines represent the first two lowest-band energy levels $\mathcal{E}_{1,2}$. (b),(c) Single-well potentials $\mathcal{V}_{1,2}(x)$, with classical turning points $\mp\bar{x}$, so that $\mathcal{V}_{1,2}(\mp\bar{x}) = \bar{E}_0$, the single-site ground state energy. The separation point x_0 is defined so that $\mathcal{V}_1(x_0) = \mathcal{V}_2(x_0) = 0$.

given by Eq. (4) for $N = 3$, can be explicitly written as

$$H_3 = \bar{E}_0 \sum_{j=1}^{3} |\Psi_j\rangle\langle\Psi_j| + \bar{\Omega}_0(|\Psi_1\rangle\langle\Psi_2| + |\Psi_2\rangle\langle\Psi_3| + \text{H.c.}). \tag{8}$$

Following the same procedure, i.e., by diagonalizing H_3 and identifying the obtained spectrum with the exact lowest-band one, we obtain

$$\begin{aligned}
\bar{E}_0 &= \frac{1}{2}(\mathcal{E}_1 + \mathcal{E}_3), \quad \bar{\Omega}_0 = \frac{1}{2\sqrt{2}}(\mathcal{E}_1 - \mathcal{E}_3),\\
\Psi_1(x) &= \frac{1}{2}\psi_1(x) + \frac{1}{\sqrt{2}}\psi_2(x) + \frac{1}{2}\psi_3(x),\\
\Psi_2(x) &= \frac{1}{\sqrt{2}}[\psi_1(x) - \psi_3(x)],\\
\Psi_3(x) &= \frac{1}{2}\psi_1(x) - \frac{1}{\sqrt{2}}\psi_2(x) + \frac{1}{2}\psi_3(x).
\end{aligned} \tag{9}$$

As in the previous case, the WFs $\Psi_{1,2,3}(x)$ are respectively localized in the left, middle, and right well, and are uniquely defined. Let us point out that our approach for a consistent determination of the tunneling Hamiltonian parameters and the related WFs can be generalized for an arbitrary number of potential wells N, regardless of the periodicity of $\mathcal{V}(x)$. Additionally, we observe that, for a *periodic* potential $\mathcal{V}(x)$, in the limit $N \to \infty$, this procedure looks similar to the method used to derive a set of localized WFs from the Bloch functions, subjected to periodic boundary conditions, through a unitary transformation. However, due to the additional "gauge freedom," the resulting WFs become strongly nonunique, so that different choices of the gauge correspond to different sets of WFs having different shapes and spreads. A widely used approach to avoid the gauge freedom consists in a proper choice of the unitary transformation of the Bloch functions that enforces the maximal localization of the WFs (see [35] for a detailed discussion). However, this procedure does not guarantee that the tunneling Hamiltonian dynamics corresponds to that obtained from the exact solution of the original multiwell Schrödinger equation.

In contrast, our approach is based on this correspondence, which allows one to uniquely construct the tunneling Hamiltonian and the WFs by assuming only the single-band approximation. Notice that the resulting WFs, although localized at the corresponding site, exhibit *tails* penetrating to neighboring sites. These tails play a crucial role in the evaluation of the nonstandard Hubbard terms, as we will show in the following. On the contrary, the condition of maximal localization of the WFs would decrease correspondingly the contribution from these tails and therefore the amplitude of the nonstandard Hubbard terms. Since our approach relates the WFs to the exact Schrödinger eigenstates, in the next section we present a consistent perturbative approach for their evaluation in terms of single-site orbitals.

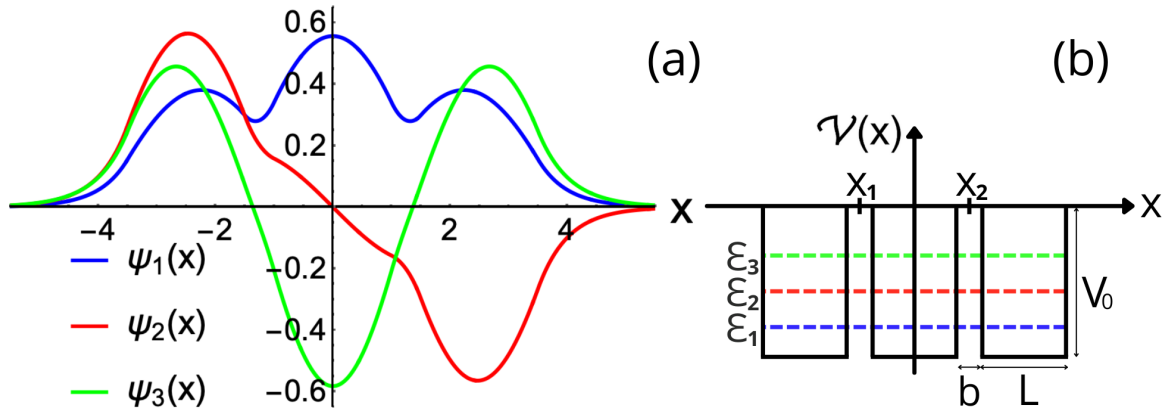

FIG. 2. (a) First three exact eigenfunctions $\psi_1(x)$ (blue curve), $\psi_2(x)$ (red curve), and $\psi_3(x)$ (green curve) of a square triple-well potential. (b) Symmetric square triple-well potential. The three wells have width L and depth V_0 and are separated by barriers of width b, where $x_{1,2}$ are the separation points. Dashed colored lines represent the first three exact energy levels of the system $\mathcal{E}_{1,2,3}$, corresponding to the eigenfunctions shown in panel (a), which read $\mathcal{E}_1 = -4.171$, $\mathcal{E}_2 = -3.897$, and $\mathcal{E}_3 = -3.545$. Parameters: $L = 2$, $b = 0.5$, and $V_0 = 5$, in arbitrary units.

III. TWO-POTENTIAL APPROACH

Let us consider the symmetric double-well potential in Fig. 1(a), given by the sum of two single-well potentials, $\mathcal{V}(x) = \mathcal{V}_1(x) + \mathcal{V}_2(x)$, such that $\mathcal{V}_1(x) = 0$ for $x \geqslant x_0$ and $\mathcal{V}_2(x) = 0$ for $x \leqslant x_0$, where $x_0 = 0$ is the separation point; see Figs. 1(b) and 1(c). The lowest eigenstates (orbitals) of the left- and right-well Hamiltonians are obtained from

$$\left(-\frac{\nabla_x^2}{2m} + \mathcal{V}_{1,2}(x)\right)\Phi_0^{(1,2)}(x) = E_0\Phi_0^{(1,2)}(x), \tag{10}$$

with the following boundary conditions:

$$\begin{aligned} &\Phi_0^{(1)}(x) \sim e^{\sqrt{-2mE_0}x} \quad \text{as } x \to -\infty, \\ &\Phi_0^{(1)}(x) = \Phi_0^{(1)}(0)e^{-\sqrt{-2mE_0}x} \quad \text{as } x \geqslant x_0, \end{aligned} \tag{11}$$

and similarly for $\Phi_0^{(2)}(x) = \Phi_0^{(1)}(-x)$. These orbitals can be used as a basis to obtain the eigenstates $\psi_{1,2}(x)$ and the WFs $\Psi_{1,2}(x) \equiv \Psi_{L,R}(x)$, through a perturbative approach. For instance, we could consider the left-well orbital $\Phi_0^{(1)}(x)$ as the unperturbed state and the right-well potential $\mathcal{V}_2(x)$ as the perturbation (or vice versa).

However, such a perturbative approach does not include a small parameter, which makes the corresponding expansion unusable. This issue can be solved by employing the TPA, which uses an alternative expansion in powers of the orbitals overlap $\beta \equiv \langle\Phi_0^{(1)}|\Phi_0^{(2)}\rangle$, a small parameter proportional to the barrier penetration coefficient

$$T_0 = \exp\left(-\int_{-\bar{x}}^{\bar{x}} |p(x')|\,dx'\right) \ll 1. \tag{12}$$

Here, $p(x)$ represents the (imaginary) momentum under the potential barrier and $\pm\bar{x}$ are the classical turning points, shown in Figs. 1(b) and 1(c) (for details, see the Supplemental Material [34]). Using this approach, we derive the tunneling Hamiltonian parameters in Eq. (7a), which read

$$\overline{E}_0 = E_0 + \mathcal{O}(\beta^2),$$

$$\overline{\Omega}_0 = \Omega_0 + \mathcal{O}(\beta^2),$$

where E_0 is given by Eq. (10), and

$$\Omega_0 = -\sqrt{\frac{2|E_0|}{m}}[\Phi_0(0)]^2 \propto T_0 \tag{13}$$

is a simplified (1D) version of the well-known Bardeen formula [36]. Similarly, we obtain

$$\mathcal{E}_{1,2} = E_\pm + \mathcal{O}(\beta^2),$$

where $E_\pm = E_0 \pm \Omega_0$. Consequently, all the parameters of the tunneling Hamiltonian are completely determined by the single-well orbitals. At first glance, we may expect to derive the eigenstates $\psi_{1,2}(x) \equiv \psi_{1,2}(E_\pm, x)$ from Eq. (7b) by replacing the WFs $\Psi_{1,2}(x)$ with the corresponding orbitals $\Phi_0^{(1,2)}(x) \equiv \Phi_0^{(1,2)}(E_0, x)$ given by Eq. (10), so that

$$\psi_{1,2}(E_\pm, x) \simeq \frac{1}{\sqrt{2}}\left[\Phi_0^{(1)}(E_0, x) \pm \Phi_0^{(2)}(E_0, x)\right]. \tag{14}$$

However, Eq. (14) exhibits an inconsistency between the energy arguments of $\psi_{1,2}(E_\pm, x)$ and $\Phi_0^{(1,2)}(E_0, x)$. To solve this issue, we introduce an energy shift in the orbital functions by replacing the ground state energy E_0 with a free parameter $E < 0$. The resulting modified orbitals $\overline{\Phi}^{(1,2)}(E, x)$ (normalized to unity) are obtained from Eq. (10) with the substitution $E_0 \to E$ and imposing the boundary condition at infinity given in Eqs. (11). However, unlike $\Phi_0^{(1,2)}(E_0, x)$, the modified orbitals $\overline{\Phi}^{(1,2)}(E, x)$ are defined respectively on two different segments

$$\mathcal{X}_1 = (-\infty, 0), \quad \mathcal{X}_2 = (0, \infty),$$

and vanish elsewhere. As a result, they are *nonoverlapping* and therefore *orthogonal*. Replacing $\Phi_0^{(1,2)}(E_0, x)$ in Eq. (14) with $\overline{\Phi}^{(1,2)}(E_\pm, x)$, we obtain

$$\psi_{1,2}(E_\pm, x) = \frac{1}{\sqrt{2}}[\overline{\Phi}^{(1)}(E_\pm, x) \pm \overline{\Phi}^{(2)}(E_\pm, x)], \tag{15}$$

which gives the *exact* result for $\psi_{1,2}(E_\pm, x)$, in contrast with Eq. (14). Indeed, the exact treatment of the Schrödinger Eq. (2) involves solving it on the two segments and combining the results by imposing the continuity condition at the separation point. This condition is automatically satisfied if $E_\pm$ are the energies of the symmetric and antisymmetric states, respectively.

Substituting Eq. (15) into Eq. (7b), we obtain the exact left- and right-well WFs, $\Psi_{L,R}(x)$, in terms of the modified orbitals:

$$\begin{aligned} \Psi_L(x) &= \tfrac{1}{2}[\overline{\Phi}_+^{(1)}(x) + \overline{\Phi}_+^{(2)}(x) + \overline{\Phi}_-^{(1)}(x) - \overline{\Phi}_-^{(2)}(x)], \\ \Psi_R(x) &= \tfrac{1}{2}[\overline{\Phi}_+^{(1)}(x) + \overline{\Phi}_+^{(2)}(x) - \overline{\Phi}_-^{(1)}(x) + \overline{\Phi}_-^{(2)}(x)], \end{aligned} \tag{16}$$

where $\overline{\Phi}_\pm^{(1,2)}(x) \equiv \overline{\Phi}^{(1,2)}(E_0 \pm \Omega_0, x)$. Expanding the modified orbitals in powers of Ω_0 and neglecting $\mathcal{O}(\Omega_0^2)$ terms (since $\Omega_0 \propto \beta \propto T_0$) we obtain

$$\overline{\Phi}_\pm^{(1,2)}(x) = \overline{\Phi}_0^{(1,2)}(x) \pm \Omega_0\,\partial_E\overline{\Phi}_0^{(1,2)}(x), \tag{17}$$

where

$$\overline{\Phi}_0^{(1,2)}(x) \equiv \begin{cases} \Phi_0^{(1,2)}(E_0, x) & \text{for } x \in \mathcal{X}_{1,2}, \\ 0 & \text{elsewhere} \end{cases} \tag{18}$$

and

$$\partial_E\overline{\Phi}_0^{(1,2)}(x) \equiv \left(\frac{\partial\overline{\Phi}^{(1,2)}(E, x)}{\partial E}\right)_{E=E_0}.$$

Substituting Eq. (17) into Eqs. (16), we get

$$\begin{aligned} \Psi_L(x) &= \overline{\Phi}_0^{(1)}(x) + \Omega_0\partial_E\overline{\Phi}_0^{(2)}(x), \\ \Psi_R(x) &= \overline{\Phi}_0^{(2)}(x) + \Omega_0\partial_E\overline{\Phi}_0^{(1)}(x), \end{aligned} \tag{19}$$

which represents our main result for the WFs. Looking at Eqs. (19), we can observe that each WF consists of two *nonoverlapping* terms, describing respectively the WF inside the respective well (first term) and its tail penetrating into the neighboring well (second term), which is $\propto \Omega_0$ and therefore much smaller than the first term. Since $\overline{\Phi}^{(1,2)}(E, x)$ are normalized to unity for any E, we can explicitly demonstrate the

orthogonality of the WFs by using

$$\partial_E \int_{-\infty}^{0} [\overline{\Phi}^{(1)}(E,x)]^2\, dx = 0,$$

so that

$$\langle \Psi_L | \Psi_R \rangle = 2\Omega_0 \int_{-\infty}^{0} \overline{\Phi}_0^{(1)}(x)\partial_E \overline{\Phi}_0^{(1)}(x)\, dx = 0. \tag{20}$$

Equation (20) represents the overlap of the orbital $\overline{\Phi}_0^{(1)}(x)$, which is nodeless, with the tail of the WF belonging to the adjacent well; see Eqs. (19). From Eq. (20), it clearly follows that the WF tail must change its sign, deeply affecting the amplitudes of the nonstandard Hubbard terms. Finally, we point out that Eqs. (19) are valid for an arbitrary multiwell system. In the next section, we exemplify this by comparing the WFs given by Eqs. (19) with the exact numerical results for a symmetric square triple-well potential.

IV. TWO-POTENTIAL APPROACH FOR A TRIPLE-WELL POTENTIAL

In this section, we explicitly demonstrate the accuracy of our analytical approach by analyzing the WFs of the symmetric square triple-well potential shown in Fig. 2(b). Specifically, we evaluate the WFs by using the TPA and we compare them with the exact WFs given by Eqs. (9), as well as with the corresponding orbital functions. For simplicity, we consider a square well potential, since its shape allows us to obtain simple analytical expressions for the WFs, which will be used for the evaluation of the nonstandard Hubbard terms, highlighting their explicit dependence on the quantum well parameters.

The triple-well spectrum, namely the eigenfunctions $\psi_k(x) \equiv \psi_k(\mathcal{E}_k, x)$ and the eigenvalues $\mathcal{E}_k$, is obtained by solving the Schrödinger Eq. (2) with boundary conditions given by Eq. (3). We focus on the three lowest-band eigenstates (with $k = 1, 2, 3$) displayed in Fig. 2(a). The corresponding exact left-, middle-, and right-well WFs $\Psi_{L,M,R}(x)$ can be obtained from the lowest-band eigenstates through Eqs. (9). On the other hand, we notice that the energy $\overline{E}_0$ in the tunneling Hamiltonian in Eq. (8) corresponds to the energy of the lowest orbital $\Phi_0(x)$ given by Eq. (10) by considering the single-well potential

$$\mathcal{V}(x) = -V_0 \quad \text{for} \quad -\frac{L}{2} < x < \frac{L}{2}.$$

Specifically, the lowest single-well orbital can be written as

$$\Phi_0(x) = \mathcal{N}_0 \begin{cases} \sqrt{1-\frac{|E_0|}{V_0}}\, e^{q_0\left(x+\frac{L}{2}\right)} & \text{for } -\infty < x < -\frac{L}{2}, \\ \cos(p_0 x) & \text{for } -\frac{L}{2} < x < \frac{L}{2}, \\ \sqrt{1-\frac{|E_0|}{V_0}}\, e^{-q_0\left(x-\frac{L}{2}\right)} & \text{for } \frac{L}{2} < x < \infty, \end{cases} \tag{21}$$

where $p_0 = \sqrt{2m(V_0 + E_0)}$, $q_0 = \sqrt{-2mE_0}$, and $\mathcal{N}_0 = \sqrt{2q_0/(2 + Lq_0)}$ is the normalization factor. As a result, the orbital functions for the triple-well system (respectively for the left, middle, and right well) read

$$\begin{aligned} \Phi_0^{(1)}(x) &\equiv \Phi_0(x + L + b), \\ \Phi_0^{(2)}(x) &\equiv \Phi_0(x), \\ \Phi_0^{(3)}(x) &\equiv \Phi_0(x - L - b). \end{aligned} \tag{22}$$

Substituting $\Phi_0(\frac{L+b}{2})$ into Eq. (13), we obtain for the tunneling energy

$$\Omega_0 = -\sqrt{\frac{2|E_0|}{m}}\mathcal{N}_0^2\left(1 - \frac{|E_0|}{V_0}\right)e^{-q_0 b}. \tag{23}$$

For the single-well parameters used in Fig. 2, solving Eq. (10) and Eq. (23) we obtain $E_0 = -3.8525$ and $\Omega_0 = -0.2216$. These values can be compared with those obtained from the exact numerical solution of the Schrödinger equation for the triple-well potential, namely $\overline{E}_0 = -3.858$ and $\overline{\Omega}_0 = -0.2215$. Their closeness confirms the high accuracy of the TPA for a consistent determination of the tunneling Hamiltonian parameters.

Finally, let us evaluate the corresponding WFs that can be obtained by extending Eqs. (19) to a triple-well system. By following the same procedure of the square double-well potential case, we construct the eigenstates $\psi_k(x)$ through the modified orbitals, with energy shift $\mathcal{E}_k - E_0 \propto \Omega_0$. We then obtain the WFs from the eigenstates $\psi_k(x)$ via the unitary transformation in Eq. (5). By expanding the resulting WFs in powers of Ω_0 up to $\mathcal{O}(\Omega_0^2)$ terms, we get a simple result representing the straightforward extension of Eqs. (19), given by

$$\begin{aligned} \Psi_L(x) &= \overline{\Phi}_0^{(1)}(x) + \Omega_0 \partial_E \overline{\Phi}_0^{(2)}(x), \\ \Psi_M(x) &= \overline{\Phi}_0^{(2)}(x) + \Omega_0\big[\partial_E \overline{\Phi}_0^{(1)}(x) + \partial_E \overline{\Phi}_0^{(3)}(x)\big], \\ \Psi_R(x) &= \overline{\Phi}_0^{(3)}(x) + \Omega_0 \partial_E \overline{\Phi}_0^{(2)}(x). \end{aligned} \tag{24}$$

As in the double-well case, $\overline{\Phi}_0^{(1,2,3)}(x)$ denote the left-, middle-, and right-well modified orbitals, respectively coinciding with $\Phi_0^{(1,2,3)}(x)$ of Eqs. (22) on the intervals $(-\infty, x_1)$, (x_1, x_2), and (x_2, ∞), and vanishing elsewhere. The separation points $x_{1,2}$ are taken at the center of the interwell barriers, as shown in Fig. 2(b).

Looking at Eqs. (24), we notice that the WFs for the triple-well system are given by the same expressions of the double-well system in Eq. (19). Indeed, the first term representing the WF inside the respective well is given by the orbital, while the second term (with derivatives) describing the WF tails penetrating to neighboring wells is proportional to Ω_0. Let us remark that the latter represents the energy shift (tunneling energy) for the *double-well* potential. Remarkably, even if the energy shift in the triple-well case is different ($\mathcal{E}_1 - E_0 = \sqrt{2}\Omega_0$), see Eqs. (9), the $\sqrt{2}$ factor cancels out during the derivation, confirming that the WF tail is always determined by the tunneling coupling to the neighboring well. A detailed derivation for a generic multiwell system will be given in a separate work.

In Fig. 3, we compare the WFs $\Psi_{L,M,R}(x)$ in Eqs. (24) obtained with the TPA (blue dashed curves) with the orbital functions $\Phi_0^{(1,2,3)}(x)$ in Eqs. (22) (black dashed curves) and the exact results in Eq. (9) obtained via numerical calculations

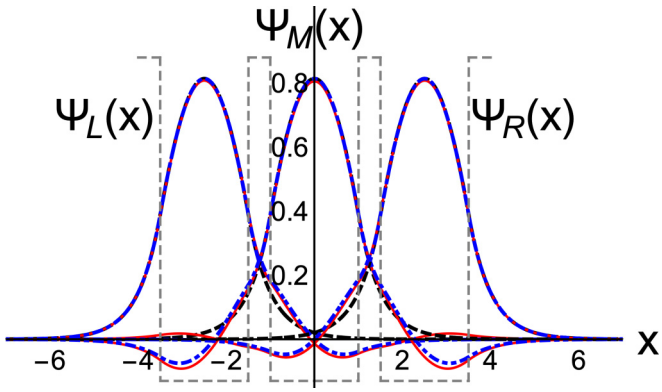

FIG. 3. Left-, middle-, and right-well WFs for the square triple-well potential shown with dashed gray lines. Red solid curves correspond to exact calculations in Eq. (9), blue dashed curves show our analytical results obtained with the TPA in Eqs. (24), and black dashed curves show the orbital functions $\Phi_0^{(1,2,3)}(x)$ in Eqs. (22). Parameters: $L = 2$, $b = 0.5$, and $V_0 = 5$, in arbitrary units.

(red solid curves). We observe that the orbitals $\Phi_0^{(1,2,3)}(x)$ provide a close approximation to the corresponding exact WFs $\Psi_{L,M,R}(x)$ within each well, despite notable differences in their tails into neighboring wells. Furthermore, the approximate results closely match the exact ones, even in the regions of the tails (beyond the respective well), underscoring the precision of the TPA. Ultimately, we notice that the tails of the WFs into the neighboring wells are less pronounced for the left and right wells compared to the middle well, due to the slightly different boundary conditions for the modified orbitals of the external wells, as described in Eqs. (11).

In the next section, we derive the nonstandard Hubbard terms using our analytical expression for the double-well WFs in Eqs. (19) and we show how these nonstandard Hubbard terms can be used to suppress single-particle tunneling in the presence of long-range interparticle interaction.

V. NONSTANDARD HUBBARD HAMILTONIAN

A. Distinguishable interacting particles in a symmetric double-well potential

The interaction between two particles in a double-well potential can be described by a two-body *repulsive* potential $V(x-y) > 0$. Since the many-body basis for two distinguishable particles is given by the tensor product of the single-particle WFs, the matrix elements of the interaction term for two distinguishable particles in the tunneling Hamiltonian basis are given by

$$V_{i'j'ij} = \int \Psi_{i'}(x)\Psi_{j'}(y)V(x-y)\Psi_i(x)\Psi_j(y)\,dx\,dy. \tag{25}$$

Here, $\Psi_i(x)$ is the WF at site $i = L, R$ of the symmetric double-well potential in Fig. 1(a). The interaction potential in Eq. (25) can be decomposed into standard and nonstandard Hubbard terms, corresponding respectively to diagonal ($ij = i'j'$) and off-diagonal ($ij \neq i'j'$) matrix elements. The Hubbard terms can be further separated into the standard Hubbard on-site interaction term $V_{iiii} \equiv U$ (for $i = j$) and the *extended* Hubbard term $V_{ijij} \equiv \overline{U}$ (for $i \neq j$) [3], respectively defined as

$$U = \int \Psi_L^2(x)V(x-y)\Psi_L^2(y)\,dx\,dy, \tag{26a}$$

$$\overline{U} = \int \Psi_L^2(x)V(x-y)\Psi_R^2(y)\,dx\,dy. \tag{26b}$$

Similarly, the nonstandard Hubbard terms can be separated into the DT (Ω_1) and PT (Ω_2) terms, with amplitudes respectively given by

$$\Omega_1 = \int \Psi_L^2(x)\Psi_L(y)V(x-y)\Psi_R(y)\,dx\,dy, \tag{27a}$$

$$\Omega_2 = \int \Psi_L(x)\Psi_L(y)V(x-y)\Psi_R(x)\Psi_R(y)\,dx\,dy. \tag{27b}$$

The physical interpretation of these terms is evident: the DT term (Ω_1) represents a single-particle hopping (e.g., $\Psi_{LL} \to \Psi_{LR}$) caused by the interaction with the nontunneling particle, while the PT term (Ω_2) describes the direct (e.g., $\Psi_{LL} \to \Psi_{RR}$) and exchange (e.g., $\Psi_{LR} \to \Psi_{RL}$) two-particle hopping. In a double-well potential, the DT term in Eq. (27a) can always be added to the single-particle tunneling, resulting in an effective tunneling $\Omega_{\rm eff} \equiv \Omega_0 + \Omega_1$ [3,5]. Therefore, in principle, the effective tunneling can be suppressed by the interaction when $\Omega_1 = -\Omega_0$.

For a repulsive *contact* interaction described by

$$V(x-y) = V_\delta\,\delta(x-y) > 0, \tag{28}$$

the DT and PT terms can be evaluated directly by substituting Eqs. (19) into Eqs. (27), obtaining

$$\Omega_1 = \Omega_0 V_\delta \int_{-\infty}^{0} \left[\overline{\Phi}_0^{(1)}(x)\right]^3 \partial_E \overline{\Phi}_0^{(1)}(x)\,dx, \tag{29a}$$

$$\Omega_2 = 2\Omega_0^2 V_\delta \int_{-\infty}^{0} \left[\overline{\Phi}_0^{(1)}(x)\partial_E \overline{\Phi}_0^{(1)}(x)\right]^2 dx. \tag{29b}$$

As expected, the DT term is proportional to Ω_0, while the PT term is proportional to Ω_0^2. From Eq. (29a), we notice that, if $\Omega_1/\Omega_0 < 0$, the effective tunneling coupling $\Omega_{\rm eff}$ could be suppressed by a sufficiently large V_δ. However, comparing Eq. (20) with Eq. (29a), we can see that this suppression cannot occur for a contact interaction. Although this can be easily checked numerically, in the following we show how these results can be obtained by a careful analysis of Eq. (29a). First, let us notice that the difference between Eq. (29a) and the orthogonality expressed in Eq. (20) lies in the third power of the orbital function $[\overline{\Phi}_0^{(1)}(x)]^3$. In the latter case, the orbital function $\overline{\Phi}_0^{(1)}(0) > 0$, while the WF tail $\Omega_0\partial_E\overline{\Phi}_0^{(1)}(x)$ changes its sign inside the integral. Since the integral of their product should be zero, both contributions should cancel each other out. On the other hand, the negative contribution to the integral in Eq. (29a) is amplified compared to the positive one, because the value of the orbital $\overline{\Phi}_0^{(1)}(x)$ decreases as $x \to 0$, where the WF tail is positive. This implies that $\Omega_1 < 0$, so that the DT term has always the same sign as Ω_0 and consequently it can only increase the effective single-particle tunneling $|\Omega_{\rm eff}|$.

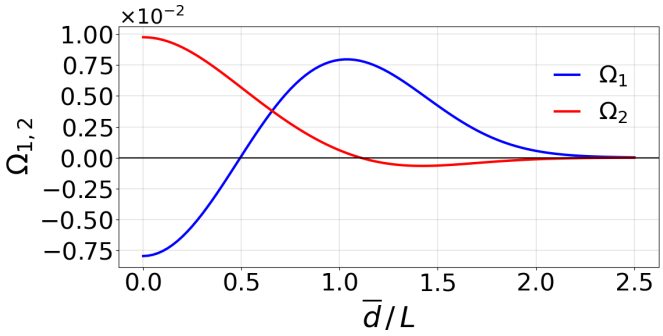

FIG. 4. DT amplitude Ω_1 (blue curve) and PT amplitude Ω_2 (red curve) as a function of the interaction range $\overline{d}$ for a symmetric square double-well potential. Parameters: $L = 2$, $b = 0.5$, $V_0 = 5$, and $\Omega_0 = -0.22$. Interaction strength $V_\delta = 1$, in arbitrary units.

This outcome undergoes a significant transformation when considering instead of a contact interaction a *long-range* one

$$V(x-y) = \begin{cases} \overline{V} & \text{for } |x-y| < \overline{d}, \\ 0 & \text{elsewhere,} \end{cases} \tag{30}$$

where $\overline{d}$ denotes the interaction range. For simplicity, in the subsequent discussion we exclusively focus on this toy-model interaction, even if similar results can be obtained using a more physically realistic *screened Coulomb* interaction, as in [37]. Moreover, this toy-model allows us to study the general behavior of the nonstandard Hubbard terms as a function of the system parameters. Indeed, from Eq. (27a), we notice that Ω_1, as a function of the interaction range, becomes positive for $\overline{d} \simeq L/2$, where L is the well width. Indeed, the main contribution to the integral in Eq. (27a) comes from $x \simeq -L/2$, at the maximum of the left-orbital function. In this case,

$$\Omega_1 \propto \int_{y_1}^{y_2} \Psi_L(y)\Psi_R(y)\,dy,$$

where $y_{1,2} = -L/2 \mp \overline{d}$. As a result, $\Omega_1 \simeq 0$ for $\overline{d} \simeq L/2$ due to orthogonality; see Eq. (20). Subsequently, Ω_1 starts to increase for $\overline{d} \gtrsim L/2$, as the long-range interaction begins to connect the central regions of the two WFs. This qualitative argument has been tested numerically in Fig. 4, where the DT and PT terms (Ω_1 and Ω_2) for two distinguishable particles in a square double-well potential with long-range interaction are shown as a function of the rescaled interaction range $\overline{d}/L$. For the sake of comparison with the contact interaction in Eq. (28), in the calculations we kept $V_\delta = 2\overline{d}\,\overline{V}$ fixed. It is clear that, in this way the results for the contact interaction are obtained in the limit $\overline{d} \to 0$ and $\overline{V} \to \infty$. The amplitudes are evaluated by substituting the exact WFs of Eq. (7b) in Eqs. (27), by using the long-range potential in Eq. (30). As expected, Ω_1 undergoes a sign change for $\overline{d} \gtrsim L/2$. Given that $\Omega_0 < 0$, see Eq. (7a), the effective single-particle tunneling Ω_{eff} can be always suppressed for some finite interaction range $\overline{d} \gtrsim L/2$ and a sufficiently large interaction strength V_δ, since $\Omega_1 \propto V_\delta$.

In the next section, we will show how PT is still possible even in the case of single-particle tunneling suppression, due to a combined action of the nonstandard Hubbard DT term and the long-range interaction.

B. Two interacting electrons with parallel spins in a square triple-well potential

As we have discussed, the suppression of single-particle tunneling coupling in the nonstandard Hubbard model arises due to the interplay of long-range repulsive electron interaction and lattice potential. In principle, we would expect that this suppression, similarly to what happens in a flat band in twisted bilayer graphene systems [37–40], disrupts the electron transport. However, instead of being suppressed, transport can still occur via PT of localized electron pairs that are not subjected to "decay" through single-electron tunneling processes [7].

One can argue that, even in the context of the standard Hubbard model, single-electron hopping in a double-well potential is suppressed for large on-site interaction (U). For this reason, it could be challenging to distinguish this suppression from the one due to the nonstandard DT term. To avoid this issue, let us consider two electrons with parallel spins so that they cannot occupy the same well due to the Pauli principle. In this case, the contribution of the long-range electron interaction in neighboring sites, $\overline{U} \ll U$, replaces the standard on-site Hubbard term U. As a result, single-electron tunneling is not suppressed by the on-site interaction, while the DT term can still induce the suppression. Even in this scenario, similarly to the double-well case, the DT term and the single-particle tunneling term sum up to give an effective single-particle tunneling term Ω_{eff}. Therefore, if Ω_0 is exactly opposite to the DT term Ω_1, the electron pair occupying two adjacent wells becomes stable and moves coherently due to the PT term.

To show this mechanism explicitly, let us consider two electrons with parallel spins in a triple-well potential, as shown in Fig. 5(a). The corresponding lowest-band Hamiltonian can be written as

$$\hat{H} = \hat{H}_3 + \hat{V}, \tag{31}$$

where $\hat{H}_3$ is the noninteracting tight-binding tunneling Hamiltonian, given by Eq. (8), while $\hat{V}$ represents the interparticle interaction term. The noninteracting Hamiltonian can be rewritten in the second quantization formalism as

$$\hat{H}_3 = E_0 \sum_{j=1}^{3} \hat{n}_j + \Omega_0(\hat{a}_L^\dagger \hat{a}_M + \hat{a}_M^\dagger \hat{a}_R + \text{H.c.}), \tag{32}$$

where $\hat{a}_j^{(\dagger)}$ destroys (creates) an electron at site $j = 1, 2, 3 \equiv L, M, R$, $\hat{n}_j = \hat{a}_j^\dagger \hat{a}_j$ is the number operator, E_0 is the site energy, and Ω_0 is the tunneling energy given by Eq. (23). Since the Hamiltonian does not contain any spin-flip terms, the number operators $\hat{n}_j$ involve only parallel spins, so that the spin indices can be omitted.

In a similar way, the interaction operator $\hat{V}$ can be written in the second quantization formalism as

$$\hat{V} = \frac{1}{2} \sum_{i'j'ij} V_{i'j'ij} \hat{a}_{i'}^\dagger \hat{a}_{j'}^\dagger \hat{a}_j \hat{a}_i, \tag{33}$$

where $V_{i'j'ij}$ is obtained by substituting in Eq. (25) the triple-well WFs $\Psi_j(x) \equiv \langle x|\hat{a}_j^\dagger|0\rangle$ given by Eqs. (9) and the long-range potential interaction of Eq. (30). Thus, considering only parallel-spin electron motion, Eq. (33) can be explicitly

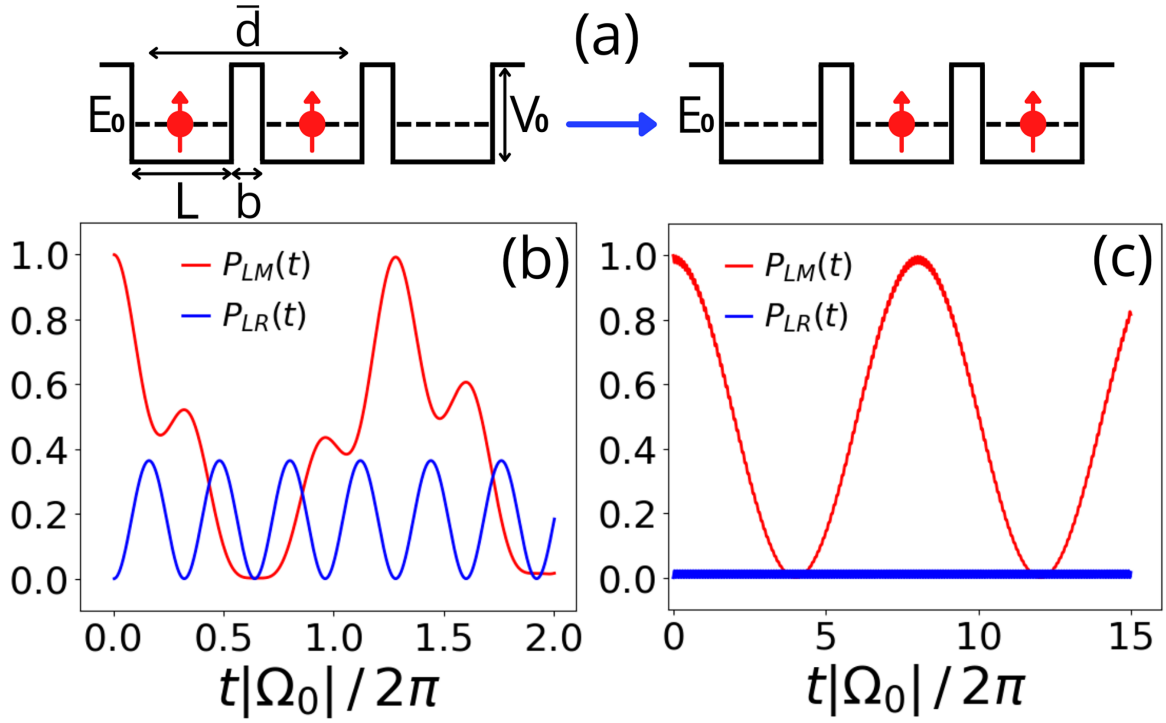

FIG. 5. (a) Coherent motion of two interacting electrons with parallel spins in a symmetric square triple-well potential, corresponding to the PT process. Black dashed lines correspond to the single-site ground state energy E_0, while $\bar{d}$ is the interaction range. (b) Occupancy probabilities $P_{LM}(t)$ (red curve) and $P_{LR}(t)$ (blue curve) for $L = 2$, $b = 0.5$, $V_0 = 5$, and $\Omega_0 \simeq -0.22$. (c) Occupancy probabilities $P_{LM}(t)$ (red curve) and $P_{LR}(t)$ (blue curve) for $L = 4$, $b = 1$, $V_0 = 5$, and $\Omega_0 \simeq -0.0167$. Interaction strength $V_\delta = 3$ and interaction range $\bar{d}/L = 2$, so that $\overline{U} \simeq 0.35$, $\Omega_1 \simeq 0.0125$, and $\Omega_2 \simeq 0.0012$ in (b) and $\overline{U} \simeq 0.19$, $\Omega_1 \simeq 0.0027$, and $\Omega_2 \simeq -6.4 \times 10^{-6}$ in (c), in arbitrary units.

written as

$$\hat{V} = \overline{U}(\hat{n}_L\hat{n}_M + \hat{n}_M\hat{n}_R) + \Omega_1(\hat{n}_L\hat{a}_M^\dagger\hat{a}_R + \hat{n}_R\hat{a}_M^\dagger\hat{a}_L + \text{H.c.}) - \Omega_2(\hat{n}_M\hat{a}_L^\dagger\hat{a}_R + \hat{n}_M\hat{a}_R^\dagger\hat{a}_L), \tag{34}$$

where $\overline{U}$ represents the nearest neighbor interaction term, obtained in the triple-well case by replacing $\Psi_R(x)$ with $\Psi_M(x)$ in Eq. (26b), so that

$$\overline{U} = \int \Psi_L^2(x)V(x-y)\Psi_M^2(y)\,dx\,dy, \tag{35}$$

while the last two terms describe respectively the DT and PT processes, with amplitudes given by

$$\Omega_1 = \int \Psi_L^2(x)\Psi_M(y)V(x-y)\Psi_R(y)\,dx\,dy, \tag{36a}$$

$$\Omega_2 = \int \Psi_L(x)\Psi_M(x)V(x-y)\Psi_M(y)\Psi_R(y)\,dx\,dy, \tag{36b}$$

where $\Omega_1 \equiv \Omega_1^{M\to R} = \Omega_1^{M\to L}$ and $\Omega_2 \equiv \Omega_2^{L\to M,M\to R} = \Omega_2^{R\to M,M\to L}$. Notice that, in our calculations, we have chosen the interaction range $\bar{d}$ in Eq. (30) so that the contribution from the next-to-nearest neighbor term can be neglected. In this way, the total Hamiltonian in Eq. (31) represents the *nonstandard* Hubbard model, whereas the *extended* Hubbard model arises simply by setting $\Omega_1 = \Omega_2 = 0$ in Eq. (34). Finally, we observe that, in the presence of long-range interaction, the DT term Ω_1 changes its sign depending on the interaction range, as illustrated in Fig. 4 for the double-well system (for the triple-well case, see Fig. S2.1 in the Supplemental Material [34]).

The effectiveness of our approach can be tested directly by studying the quantum dynamics of the system. In particular, let us consider as initial condition two electrons occupying two neighboring wells $\bar{j}$ and $\bar{j}'$. Their time-dependent wave function can always be written as

$$|\Psi^{(\bar{j}\,\bar{j}')}(t)\rangle = \sum_{j<j'} b_{jj'}^{(\bar{j}\,\bar{j}')}(t)\,\hat{a}_j^\dagger\hat{a}_{j'}^\dagger\,|0\rangle\,, \tag{37}$$

where $j, j' = L, M, R$, while the upper indices $(\bar{j}\,\bar{j}')$ label the initial state. Specifically, let us choose $\bar{j} = L$ and $\bar{j}' = M$, so that the left and middle wells are initially occupied. Then, Eq. (37) can be explicitly written as

$$|\Psi^{(LM)}(t)\rangle = \big[b_{LM}^{(LM)}(t)\,\hat{a}_L^\dagger\hat{a}_M^\dagger + b_{LR}^{(LM)}(t)\,\hat{a}_L^\dagger\hat{a}_R^\dagger + b_{MR}^{(LM)}(t)\,\hat{a}_M^\dagger\hat{a}_R^\dagger\big]\,|0\rangle\,. \tag{38}$$

By substituting Eq. (38) into the time-dependent Schrödinger equation

$$i\partial_t\,|\Psi^{(\bar{j}\,\bar{j}')}(t)\rangle = (\hat{H}_3 + \hat{V})\,|\Psi^{(\bar{j}\,\bar{j}')}(t)\rangle\,, \tag{39}$$

we obtain the following equations of motion:

$$i\dot{b}_{LM}^{(LM)}(t) = (2E_0 + \overline{U})b_{LM}^{(LM)}(t) + (\Omega_0 + \Omega_1)b_{LR}^{(LM)}(t) + \Omega_2 b_{MR}^{(LM)}(t),$$

$$i\dot{b}_{LR}^{(LM)}(t) = 2E_0 b_{LR}^{(LM)}(t) + (\Omega_0 + \Omega_1)\big[b_{LM}^{(LM)}(t) + b_{MR}^{(LM)}(t)\big],$$

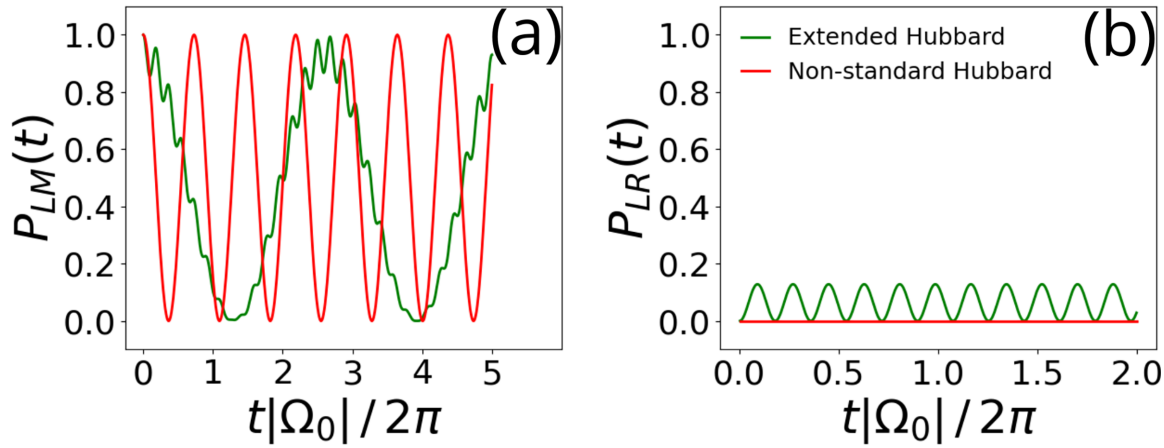

FIG. 6. (a) Occupancy probabilities $P_{LM}(t)$ and (b) occupancy probabilities $P_{LR}(t)$ obtained with the nonstandard Hubbard model (red curves) and the extended Hubbard model (green curves), for the case of complete single-particle tunneling suppression. Parameters: $L = 2$, $b = 0.1$, $V_0 = 1.1$, and $\Omega_0 \simeq -0.32$. Interaction strength $V_\delta = 22$ and interaction range $\overline{d}/L = 2$, so that $\overline{U} \simeq 1.54$, $\Omega_1 \simeq -\Omega_0$, and $\Omega_2 \simeq 0.22$, in arbitrary units.

$$i\dot{b}_{MR}^{(LM)}(t) = (2E_0 + \overline{U})b_{MR}^{(LM)}(t) + (\Omega_0 + \Omega_1)b_{LR}^{(LM)}(t) + \Omega_2 b_{LM}^{(LM)}(t). \quad (40)$$

Looking at Eqs. (40), we notice that the DT term Ω_1 appears only together with the single-particle tunneling Ω_0, thus giving rise to an effective single-particle tunneling $\Omega_{\rm eff} = \Omega_0 + \Omega_1$ [3–5]. Equations (40) can be integrated numerically to obtain the occupancy probabilities for all sites of the triple-well system as a function of time. Specifically, the probability to find the two electrons in the wells j, j' is defined as

$$P_{jj'}(t) = \langle \Psi^{(LM)}(t)|\, \hat{n}_j \hat{n}_{j'}\, |\Psi^{(LM)}(t)\rangle = \left|b_{jj'}^{(LM)}(t) - b_{j'j}^{(LM)}(t)\right|^2, \quad (41)$$

while the probability to find one electron occupying the well j is defined as

$$P_j(t) = \sum_{j' \neq j} \left|b_{jj'}^{(LM)}(t)\right|^2. \quad (42)$$

In Figs. 5(b) and 5(c), we show the probabilities $P_{LM}(t)$ and $P_{LR}(t)$, derived from Eq. (41), for two different geometries of the triple-well system at some fixed interparticle interaction strength. Particularly, in Fig. 5(c), we adjust the geometry of the system (by enlarging the well and barrier widths) to produce a significant suppression of $P_{LR}(t)$, if compared with that in Fig. 5(b). This suppression suggests the emergence of a propagating correlated electron pair within the system, showing that single-particle tunneling can be suppressed induced by modifying the well parameters. Note that a similar suppression is also observable within the extended Hubbard model framework. Specifically, it is easy to show that the suppression of $P_{LR}(t)$ in the extended Hubbard model occurs when $\overline{U} \gg \Omega_0$ (for details, see the Supplemental Material [34]).

Clearly, the nonstandard and extended Hubbard model diverge significantly when complete suppression of single-particle tunneling occurs, i.e., for $\Omega_1 = -\Omega_0$. To show this explicitly, we adjust the geometry of the system and the interaction strength to achieve complete suppression of single-particle tunneling $\Omega_{\rm eff}$. Results are shown in Fig. 6 for both nonstandard (red curves) and extended (green curves) Hubbard models. As one can see, notable distinctions between the two models' predictions exist. Specifically, the extended Hubbard model predicts a small, but not zero, amplitude for $P_{LR}(t)$ [see Fig. 6(b)], as well as a smaller oscillation frequency of $P_{LM}(t)$ compared to the nonstandard Hubbard model [see Fig. 6(a)]. Given that in the nonstandard Hubbard model the single particle tunneling is suppressed, the enhanced transport efficiency, signaled by the high frequency of oscillations of $P_{LM}(t)$, is due to the presence of the PT term.

Finally, one may wonder what is the region of parameters in which the nonstandard and extended Hubbard model give approximately similar outcomes. Within the validity of the single-band approximation, a glance at Eq. (40) reveals that the two Hubbard models are expected to give close results when the Ω_1 and Ω_2 terms become negligible compared to Ω_0, namely for sufficiently weak interaction strength. A detailed comparison between the two Hubbard models, as well as a comparison with our analytical approach, is reported in the Supplemental Material [34].

VI. CONCLUSIONS

In conclusion, we have explored the conditions governing the suppression of single-particle tunneling coupling in periodic systems, within the framework of a nonstandard Hubbard model, including density-induced tunneling and pair tunneling terms. Our findings demonstrate that such suppression cannot occur with a conventional contact repulsive interaction, but only in the presence of a long-range repulsive interaction. A better understanding of the mechanism underlying the suppression of the single-particle tunneling could be a significant issue in the theory of quantum transport in correlated systems. Indeed, as we have shown here, see Fig. 6, in the presence of single-particle tunneling suppression the dynamics is dominated by pair tunneling, which enhances the transport efficiency.

The consequences of these effects are far reaching, since single-particle tunneling suppression and pair tunneling

dominated dynamics may lead to transport regimes characterized by efficient and robust electron pair transport. Indeed, within the nonstandard Hubbard model considered here, increasing the interaction strength not only suppresses single-particle tunneling but also enhances pair tunneling, introducing a competition between these two effects. Such interplay may lead to nontrivial transport regimes that could potentially expand the paradigm of Mott-insulator transitions [41] beyond the standard Hubbard model. In the future, we plan to investigate the impact of the effects unveiled in this manuscript in lattice models of different dimensions.

ACKNOWLEDGMENTS

F.B., M.Z., and G.L.C. acknowledge the support of the Iniziativa Specifica INFN-DynSysMath. This work has been financially supported by the Catholic University of Sacred Heart and by M.I.U.R. within Project No. PRIN 20172H2SC4. M.Z. acknowledges the Ermenegildo Zegna's Group for financial support. S.G. would like to thank Y. Oreg and E. Berg for helpful discussions and suggestions. We also thank S. Mailoud and G. Farinacci for discussions and for their valuable contribution at the initial stage of this work.

[1] J. Hubbard, Electron correlations in narrow energy bands, Proc. R. Soc. Lond. A **276**, 238 (1963).
[2] S. Fölling, S. Trotzky, P. Cheinet, M. Feld, R. Saers, A. Widera, T. Müller, and I. Bloch, Direct observation of second-order atom tunnelling, Nature (London) **448**, 1029 (2007).
[3] O. Dutta, M. Gajda, P. Hauke, M. Lewenstein, D.-S. Lühmann, B. A. Malomed, T. Sowiński, and J. Zakrzewski, Non-standard hubbard models in optical lattices: a review, Rep. Prog. Phys. **78**, 066001 (2015).
[4] O. Jürgensen, K. Sengstock, and D.-S. Lühmann, Density-induced processes in quantum gas mixtures in optical lattices, Phys. Rev. A **86**, 043623 (2012).
[5] O. Jürgensen, F. Meinert, M. J. Mark, H.-C. Nägerl, and D.-S. Lühmann, Observation of density-induced tunneling, Phys. Rev. Lett. **113**, 193003 (2014).
[6] S. A. Gurvitz, Two-electron correlated motion due to coulomb repulsion, arXiv:cond-mat/0203545.
[7] A. J. Leggett, *Quantum Liquids: Bose Condensation and Cooper Pairing in Condensed-Matter Systems* (Oxford University Press, Oxford, 2006), p. 335.
[8] J. E. Hirsch and F. Marsiglio, Superconducting state in an oxygen hole metal, Phys. Rev. B **39**, 11515 (1989).
[9] R. Strack and D. Vollhardt, Hubbard model with nearest-neighbor and bond-charge interaction: Exact ground-state solution in a wide range of parameters, Phys. Rev. Lett. **70**, 2637 (1993).
[10] I. N. Karnaukhov, Model of fermions with correlated hopping (integrable cases), Phys. Rev. Lett. **73**, 1130 (1994).
[11] J. de Boer, V. E. Korepin, and A. Schadschneider, η pairing as a mechanism of superconductivity in models of strongly correlated electrons, Phys. Rev. Lett. **74**, 789 (1995).
[12] G. I. Japaridze and A. P. Kampf, Weak-coupling phase diagram of the extended hubbard model with correlated-hopping interaction, Phys. Rev. B **59**, 12822 (1999).
[13] A. Anfossi, P. Giorda, A. Montorsi, and F. Traversa, Two-point versus multipartite entanglement in quantum phase transitions, Phys. Rev. Lett. **95**, 056402 (2005).
[14] A. Dobry and A. A. Aligia, Quantum phase diagram of the half filled hubbard model with bond-charge interaction, Nucl. Phys. B **843**, 767 (2011).
[15] A. Montorsi, U. Bhattacharya, D. González-Cuadra, M. Lewenstein, G. Palumbo, and L. Barbiero, Interacting second-order topological insulators in one-dimensional fermions with correlated hopping, Phys. Rev. B **106**, L241115 (2022).
[16] A. A. Aligia, A. Anfossi, L. Arrachea, C. Degli Esposti Boschi, A. O. Dobry, C. Gazza, A. Montorsi, F. Ortolani, and M. E. Torio, Incommmensurability and unconventional superconductor to insulator transition in the hubbard model with bond-charge interaction, Phys. Rev. Lett. **99**, 206401 (2007).
[17] J. E. Hirsch, Electron- and hole-hopping amplitudes in a diatomic molecule, Phys. Rev. B **48**, 3327 (1993).
[18] R. Ma, M. E. Tai, P. M. Preiss, W. S. Bakr, J. Simon, and M. Greiner, Photon-assisted tunneling in a biased strongly correlated bose gas, Phys. Rev. Lett. **107**, 095301 (2011).
[19] F. Meinert, M. J. Mark, K. Lauber, A. J. Daley, and H.-C. Nägerl, Floquet engineering of correlated tunneling in the bose-hubbard model with ultracold atoms, Phys. Rev. Lett. **116**, 205301 (2016).
[20] F. Görg, M. Messer, K. Sandholzer, G. Jotzu, R. Desbuquois, and T. Esslinger, Enhancement and sign change of magnetic correlations in a driven quantum many-body system, Nature (London) **553**, 481 (2018).
[21] A. Knothe and G. Burkard, Extended hubbard model describing small multi-dot arrays in bilayer graphene, arXiv:2401.09898.
[22] I. Affleck and J. B. Marston, Large-n limit of the heisenberg-hubbard model: Implications for high-T_c superconductors, Phys. Rev. B **37**, 3774 (1988).
[23] V. F. Gilmutdinov, M. A. Timirgazin, and A. K. Arzhnikov, Interplay of magnetism and superconductivity in 2D extended hubbard model, J. Magn. Magn. Mater. **560**, 169605 (2022).
[24] W.-C. Chen, Y. Wang, and C.-C. Chen, Superconducting phases of the square-lattice extended hubbard model, Phys. Rev. B **108**, 064514 (2023).
[25] G. D. Adebanjo, J. P. Hague, and P. E. Kornilovitch, Ubiquity of light small pairs in hubbard models with long range hoppings and interactions, Phys. Lett. A **507**, 129474 (2024).
[26] S. Kundu and D. Sénéchal, CDMFT+HFD: an extension of dynamical mean field theory for nonlocal interactions applied to the single band extended Hubbard model, arXiv:2310.16075.
[27] K. Wrześniewski, T. Ślusarski, and I. Weymann, Nonmonotonic buildup of spin-singlet correlations in a double quantum dot, Phys. Rev. B **108**, 144307 (2023).
[28] P. Frey, L. Hackl, and S. Rachel, Hilbert space fragmentation and interaction-induced localization in the extended fermi-hubbard model, Phys. Rev. B **106**, L220301 (2022).
[29] A. Nico-Katz, G. Jaliel, P. Atkinson, T. A. Mitchell, D. A. Ritchie, C. G. Smith, and S. Bose, Identifying many-body localization in realistic dot arrays, arXiv:2301.08246.

[30] D.-S. Lühmann, O. Jürgensen, and K. Sengstock, Multi-orbital and density-induced tunneling of bosons in optical lattices, New J. Phys. **14**, 033021 (2012).

[31] S. A. Gurvitz and G. Kalbermann, Decay width and the shift of a quasistationary state, Phys. Rev. Lett. **59**, 262 (1987).

[32] S. A. Gurvitz, Novel approach to tunneling problems, Phys. Rev. A **38**, 1747 (1988).

[33] S. A. Gurvitz, P. B. Semmes, W. Nazarewicz, and T. Vertse, Modified two-potential approach to tunneling problems, Phys. Rev. A **69**, 042705 (2004).

[34] See Supplemental Material at http://link.aps.org/supplemental/10.1103/PhysRevB.109.195137 for the two-potential approach to the bound-state spectrum, the Bardeen formula, the exact equations of motion of two electrons in a symmetric triple-well potential, the unitary transformation to diagonalize the tight-binding tunneling Hamiltonian for the double-well and triple-well potential cases, the behavior of the next-to-nearest neighbor interaction, DT and PT terms as a function of the interaction range for the triple-well case, a detailed comparison between the extended Hubbard model, the nonstandard Hubbard model, the analytical approach, and which includes Ref. [42].

[35] N. Marzari, A. A. Mostofi, J. R. Yates, I. Souza, and D. Vanderbilt, Maximally localized Wannier functions: Theory and applications, Rev. Mod. Phys. **84**, 1419 (2012).

[36] J. Bardeen, Tunnelling from a many-particle point of view, Phys. Rev. Lett. **6**, 57 (1961).

[37] D. D. Vu and S. Das Sarma, Moiré versus mott: Incommensuration and interaction in one-dimensional bichromatic lattices, Phys. Rev. Lett. **126**, 036803 (2021).

[38] R. Bistritzer and A. H. MacDonald, Moiré bands in twisted double-layer graphene, Proc. Natl. Acad. Sci. USA **108**, 12233 (2011).

[39] S. M. Chan, B. Grémaud, and G. G. Batrouni, Pairing and superconductivity in quasi-one-dimensional flat-band systems: Creutz and sawtooth lattices, Phys. Rev. B **105**, 024502 (2022).

[40] Y. Cao, V. Fatemi, S. Fang, K. Watanabe, T. Taniguchi, E. Kaxiras, and P. Jarillo-Herrero, Unconventional superconductivity in magic-angle graphene superlattices, Nature (London) **556**, 43 (2018).

[41] X.-F. Zhou, Y.-S. Zhang, and G.-C. Guo, Pair tunneling of bosonic atoms in an optical lattice, Phys. Rev. A **80**, 013605 (2009).

[42] D. J. Thouless, *The Quantum Mechanics of Many-body Systems* (Academic Press, New York, 1961).